Osman *et al. J Pure Appl Microbiol,* **13**(**2**), 767-778 | June 2019
Article 5559 | https://dx.doi.org/10.22207/JPAM.13.2.12

Print ISSN: 0973-7510; E-ISSN: 2581-690X

RESEARCH ARTICLE OPEN ACCESS

Photocatalytic Bacterial Disinfection using Ag^{o}/Ag^{+1} Immobilized on CNT Modified TiO_2 Nanomaterials

Gamal Osman[1,2,3], Mohamed M. Mohamed[4]* and Khalid S. Khairou[5]

[1]Department of Biology, Faculty of Applied Sciences, Umm Al Qura University, Makkah- 21955, Kingdom of Saudi Arabia. [2]Agricultural Genetic Engineering Research Institute (AGERI), Giza, Egypt. [3]Research Laboratories Center, Faculty of Applied Science, Umm Al-Qura University, Mecca, Saudi Arabia. [4]*Department of Chemistry, Faculty of Science, Benha University, Benha- 13518, Egypt. [5]Department of Chemistry, Faculty of Applied Sciences, Umm Al Qura University, Makkah - 21955, Kingdom of Saudi Arabia.

Abstract

Different loading of Ag nanoparticles (2 and 6%) modified TiO2 synthesized by employing polymeric template; comprises of polyvinyl alcohol and polyethylene glycol (Tev), were utilized to react hydrothermally (433 K for 48 h) with functionalized SWCNT and MWCNT. Several characterization techniques, including UV-visible diffuse reflectance spectroscopy, X-ray diffraction, HRTEM-ASED, and N2 sorptiometry were utilized for obtaining information about surface texturing, morphology, optical properties and crystalline phases. The synthesized photocatalysts were tested for their antibacterial activity against Escherichia coli (Gram negative bacterium) and Staphylococcus aureus (Gram positive bacterium) through agar well diffusion method under visible light irradiation (λ > 450 nm, 60 mWcm-2). It has been revealed that the photocatalyst TevAg6-SWCNT exhibited the maximum lethal action thereby inhibiting the growth of bacteria as compared to rest of the catalysts; this was due to increase in surface area value with delay in electrons and holes recombination as well as the diameter of Ago nanoparticles which was reduced to 3 nm. It has been evidenced that the nanocomposites attack mechanism on while disinfecting bacteria indicates the formation of O2•− and ·OH radicals, those played significant role in inactivation of cellular process. The TEM images revealed the role of Ag+ ions, and the presence of TevAg6-SWCNT were thoroughly studied and correlated to identify the disinfection mechanisms induced through irradiation of visible light.

Keywords: Ag/TiO_2-CNTs nanocomposites, Bacterial disinfection; DNA damage; Surface active species, morphology change.

***Correspondence:** mohmok2000@yahoo.com

(Received: 12 March 2019; accepted: 07 May 2019)

Citation: Gamal Osman, Mohamed M. Mohamed and Khalid S. Khairou, Photocatalytic Bacterial Disinfection using Ag^{o}/Ag^{+1} Immobilized on CNT Modified TiO_2 Nanomaterials, *J Pure Appl Microbiol*., 2019; **13**(**2**):767-778. doi: 10.22207/JPAM.13.2.12

INTRODUCTION

At present time, Carbon nanotubes (CNTs) have attained noteworthy importance because of their remarkable electrical, mechanical, magnetic properties, high surface areas and good chemical stability[1-2]. The TiO_2 is widely used as a photosensitizer to tackle various environmental issues[3-5]. Inefficient photocatalytic activity has however; the application of TiO_2 has been restricted in practical water treatment[6-8] because it's shows activity under the exposure of ultraviolet rays. CNTs and TiO_2 nanocomposites exhibit distinctive properties like high adsorption capacity, large surface area, as well as capable of growing in their photoassisted reactions that arise under visible light conditions because of this they have gained significant importance[9-10]. The anchoring of TiO_2 on nanocarbons obstructs recombination of electron–hole at TiO_2–CNT boundaries and therefore results in superior photocatalyic performances as compared to individual analogue counterparts[11-12].On the other hand, the morphological and structural properties of CNTs helps them to be function as specific templates in the fabrication of metal nanoparticle-CNTs composite[13-14]. From previous studies it has been found that Ag incorporated CNTs showed high electro catalytic activity towards oxidation of hydrazine[15]. In contrast, the photocatalytic activity of Ag/TiO_2 towards reduction of 4-nitrophenol was also accomplished at the interface of TiO_2 phases via the existence of Ago/Ag+ species[16-17]. Nowadays, resistance by pathogenic microorganisms towards commercially available antimicrobials has been increased at an incredible rate[18]. Accordingly, there has been an upsurge for Ag containing compounds to work as antibacterial and antifungal based on their silver nanoparticles properties[19-21]. At regular basis of life, peoples are often infected by pathogenic microorganisms including bacteria, molds, viruses, etc. Over the last few years, researchers have been synthesized efficient antibacterial materials composed of different natural and inorganic substrates[22-25]. Furthermore, Ag-NPs have the ability to bind the bacterial cell DNA and thus halting its replication machinery[26] or also targets ribosome of bacteria and inhibits translation process[27-28]. Different techniques have been used for the synthesis of Ag-NPs like reduction of silver ions through chemical means; with or without capping agents, photo reduction in reverse micelles and decomposition in organic solvents thermally[2-30]. However, the mentioned methods involve the usage of toxic and dangerous chemicals that may create biological and environmental hazards[31]. In the present scenario, the antibacterial activities of the Ag/TiO_2-CNT composites synthesized according to increased visible light harvesting capability, decrease in aggregation of Ag with taking the benefit of high surface to volume ratio are along their effects on bacterial DNA using model cell types: Escherichia coli and Staphylococcus aureas were also investigated For the manufactured CNT/TiO_2 and Ag-CNT/TiO_2 composites optical, morphological characteristics and structural variations were examined. The synthesized photocatalysts were characterized by means of X-ray diffraction (XRD), energy dispersive X-ray (EDX), transmission electron microscopy (TEM), N2 sorptiometry, FTIR, Photoluminescence, Raman and UV-vis diffuse reflectance spectroscopic techniques. The underlying mechanism that was taking part in photocatalytic disinfection process was investigated through measuring protein separation, K+ leakage and bacterial TEM images sticked on the composite surfaces.

MATERIALS AND METHODS

Catalyst preparation

In the following procedure, TiO_2 nanoparticles were fabricated by self-assembly method. Briefly, Polyethylene glycol ($HO(CH_2CH_2O)$ nH-0.01 M) and polyvinyl-alcohol (CH_2-CH(OH) n-0.01M) were thoroughly mixed in minimum amount of water (15 ml) and at a weight ratio of 7:3. Titanium iso-propoxide ($Ti(OCH(CH_3)2$)4-29.3 ml) has been added to the above mentioned mixture by stirring vigorously at room temperature for half an hour. The resulting mixture was transformed into Teflon- lined autoclave followed by 48 h hydrothermal treatment at 393 K. The product was recovered through centrifugation after hydrothermal treatment and later it was washed with deionised water. For the removal of copolymer template, the solid was dried at 333 K overnight and then calcined in air at 673 K for 6 h. This sample has been referred to as Tev. The Tev catalyst was, therefore suspended in mixture of ethanol-water individually and left

under stirring for 2 h. This combination was poured into ethanol dissolved SWCNT to make final ratio of 20% SWCNT to Tev, and then it was sonicated for about 1.5 h at 313 K. It's then left at room temperature for overnight stirring and resultant mixture was poured into a Teflon lined autoclave for 48 h followed by heating at 433 K under autogeneous pressure. Finally, it was filtered, washed with absolute ethanol and distilled water, dried overnight at 373 K and then calcined for 4 h at 673 K to be called as Tev-SWCNT.

To prepare silver containing catalysts, different weight percentages of Ag at a ratio of 2% or 6% were admitted before the addition of titanium iso-propoxide to preparing samples referred as $TevAg_2$ and $TevAg_6$. Accordingly, in a mixture of ethanol-water, $TevAg_2$ and $TevAg_6$ catalysts were dissolved individually and left under 2 h stirring. The obtained mixtures were poured into ethanol suspension of MWCNT and SWCNT to give ratios consisting of 20% MWCNT&SWCNT compared to Tev and then sonicated for 1.5 h at 313 K. Afterwards, the mixtures were poured into autoclaves and heated at 433 K for 48 h under auto-geneous pressure. The mixtures were finally referred to as $TevAg_2$-SWCNT, $TevAg_2$-MWCNTand $TevAg_6$-SWCNT.

Characterization of Catalyst

X-ray diffraction measurements were performed by using X–Ray Diffraction (XRD) spectrometer Model XRD 8030 from Jeol co., Japan. The morphological characteristics of the nanostructured composites were examined by using high resolution transmission electron microscopy (HRTEM) with an accelerating voltage of 200 kV, obtained from Tecnai G2 supper twin USA. The elemental composition of the composite sample was determined by energy-dispersive X-ray attached to the TEM equipment. The FTIR absorption spectra of the samples were recorded in the range of 400-1000 cm^{-1} using a Perkin-Elmer instrument (Spectrum GX), made in USA. Nitrogen adsorption measurements were performed for surface area in a porosity analyzer Micromeritics ASAP 2020. Diffuse Reflectance Ultraviolet–visible spectroscopy (UV–vis DRS) of powder samples was carried out using a PerkinElmer Lamda-900 spectrophotometer. The edge energy (Eg) for allowed transitions was determined by finding the intercept of the straight line in the low-energy rise of the plot of [F(R)hυ]2vs hυ, where hυ is the incident photon energy. The PL spectra were recorded by photoluminescence (PL) spectrometer (Spectro Fluorescence JASCO fp-6200) using 290 nm as a wavelength of excitation.

Antibacterial test

The gram positive bacteria S. aureus and gram negative bacteria E. coli maintained on nutrient agar (pH 6.8) were subcultured, grown and stored at 4°C. For the experimental analysis, a single isolated colony of each bacterium was inoculated into 10 ml of LB broth and incubated at 37°C overnight with shaking at 200 rpm. The optical density of the overnight grown bacterial culture was adjusted to 0.5 by spectrophotometer and the culture was diluted to give a final working concentration of 1x106CFU/ml with LB broth.

Agar well Diffusion Assay

The susceptibility of the nanoparticles solutions were determined at100µg/ml and 50µg/ml by pouring them into the well at the core in all plates having the lawn of bacteria strain. Afterwards, the plates were incubated at 37°C for 24 h, and diameter of growth inhibition was measured. As a negative control, distilled water without test compounds addition was taken. Antibiotics (vancomycin for gram positive bacteria and amikacin for gram negative bacteria [32]) were used as positive control in the agar disk diffusion method, and resulting inhibition zone diameter around each disk (in mm) was determined.

Bacterial susceptiblity towards nanocamposites

The bacterial cultures were incubated at 37°C for 24 hr under aerobic condition. Optical density (OD) of bacterial culture was measured at 600 nm with a Hitachi spectrophotometer (type 124). The instrument was manufactured by Vilber Lourmat-France, equipped with a high pressure Hg lamp (125 W) along with special UV cut off filter having wavelength(λ)> 450nm; providing the source of visible light. It gives the working distance of 30 cm with an average light intensity of 60 mWcm-2 .

Isolation of genomic DNA

Genomic DNA was isolated as described elsewhere[33]. Five random oligonucleotide primers used in the experiment includes OPA9, OPB7, OPB17, OPC13 and OPE19. Premiers were synthesized at Operon technologies, Alameda, USA (Table S- see supporting information). The

PCR products were separated on 1.4% (RAPD) Agarose gel in 1x TAE buffer containing 0.1 µgml^{-1} of ethidium bromide for about 2 hrs at 80 V. Gel was photographed under UV light with Trackt el GDS-2 gel documentation system.

RESULTS AND DISCUSSION

XRD investigation

The XRD patterns of TevAg$_2$-inset- are shown in Fig. 1, confirms the peaks of anatase (JCPDS 21-1272) peaks obtained as main phase while rutile (JCPDS 21-1276) corresponds to minor one. Incorporation of Ag at a loading of 2% decreases the anatase ratio into 90% in TevAg$_2$. At 2θ =32° very small line was also found and ascribed to Ag$_2$O species[34]. The pattern of Tev-SWCNT had no impact on the structure of Tev but the anatase was affected (101) plane. Whereas, the pattern of TevAg$_2$-SWCNT exhibits reduction in broadness and intensity for the same plane proposing superimposing of (1 0 1) plane of TiO$_2$ over (0 0 2) plane of graphitic carbons. In addition to this, the diffraction of TevAg6-SWCNT showed characteristic peaks at 38°(111), 44◦(200) and 64.4°(220);ascribed to the face centred cubic (fcc) of Ago nanoparticles (JCPDS, File No. 4-0783), together with a small peak at 2θ=32◦of Ag$_2$O. Likewise, the TevAg$_2$-MWCNT catalyst encourages the appearance of rutile peaks; not detected in Tev-SWCNT, beside Ago nanoparticles and Ag$_2$O moieties.

Surface properties

The pure Tev-SWCNT and Ag containing nanocomposites were examined for N$_2$ adsorption isotherms that is depicted in Fig. S1. According to IUPAC classification, the adsorption-desorptionisothermsare belong to Type IV. Compared to these-prepared Tev-SWCNT, the hysteresis loop of TevAg$_2$-SWCNT shows a wider relative pressure range (0.4–1.0) and larger

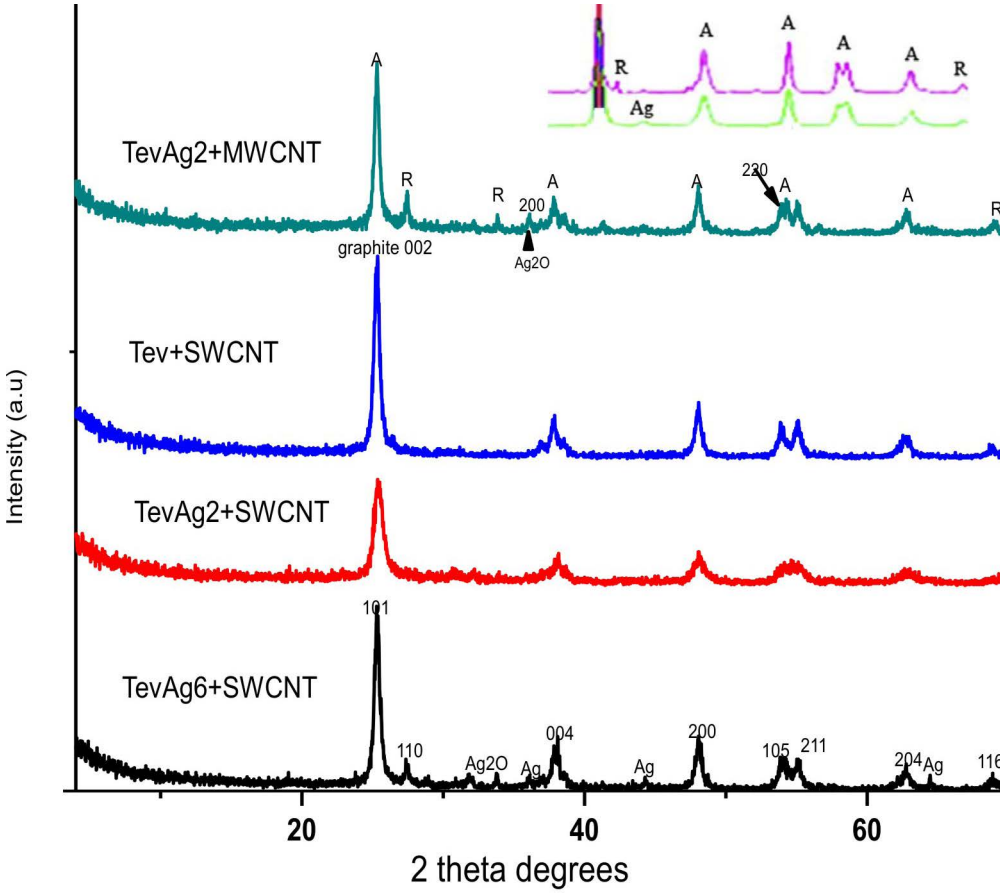

Fig.1. XRD patterns of TNT-SWCNT, TevAg2-SWCNT, TevAg2-MWCNT and TevAg6-SWCNT.

hysteresis area proposing that Ag nanoparticles results in the enhancement in progression of microporosities. This is confirmed from increasing the surface area and decreasing the pore volume values of TevAg2-SWCNT (97.5 m^2/g, 0.132 cc/g) compared with that of Tev-SWCNT (86.2 m^2/g, 0.152 cc/g). These values are reduced in case of $TevAg_6$-SWCNT (81.0 m^2/g, 0.12 cc/g),suggesting the deposition of Ag nanoparticles deep inside the TiO_2 pores. The PSD of the Tev-SWCNT sample was in the 1.0–4.0 nm range, whereas it was narrowed for Ag containing composites to be in the 1.4-3.0 nm range. $TevAg_6$-SWCNT showed narrowing of the PSD to be mainly around 2 nm; lower limit of mesopores, while in case of $TevAg_2$-SWCNT, it was about 2 and 3 nm .

The Transmission electron microscopy (TEM) morphologies of both free Ag as well as Ag confined Tev-SWCNT(MWCNT) nanocomposites are depicted in figure 2 .The Tev-SWCNT synthesized by self assembly method represents diameter of CNTs in the range of 12–25 nm while that of TiO2 nanoparticles exhibit 7–18 nm range width. The images showed the presence of TiO_2 nanoparticles, which are coated with some parts of CNT. The insets image showed the corresponding selected area electron diffraction (SAED) patterns. It also demonstrated that the CNT diffraction spots have been overloaded by the diffraction rings of TiO_2 nanoparticles. The SAED patterns revealed that the spherical rings lined up with planes of CNT (002), anatase (101), (004), (200), (105) and rutile (110) phases. The TEM images of $TevAg_2$-SWCNT shows that the average diameter of TiO_2 and CNT were 12 nm and 10 nm, respectively whereas Ag nanoparticles exhibit 5 nm diameter. In both samples of $TevAg_6$-SWCNT and $TevAg_2$-MWCNT a significant decrease in CNT thickness via displaying

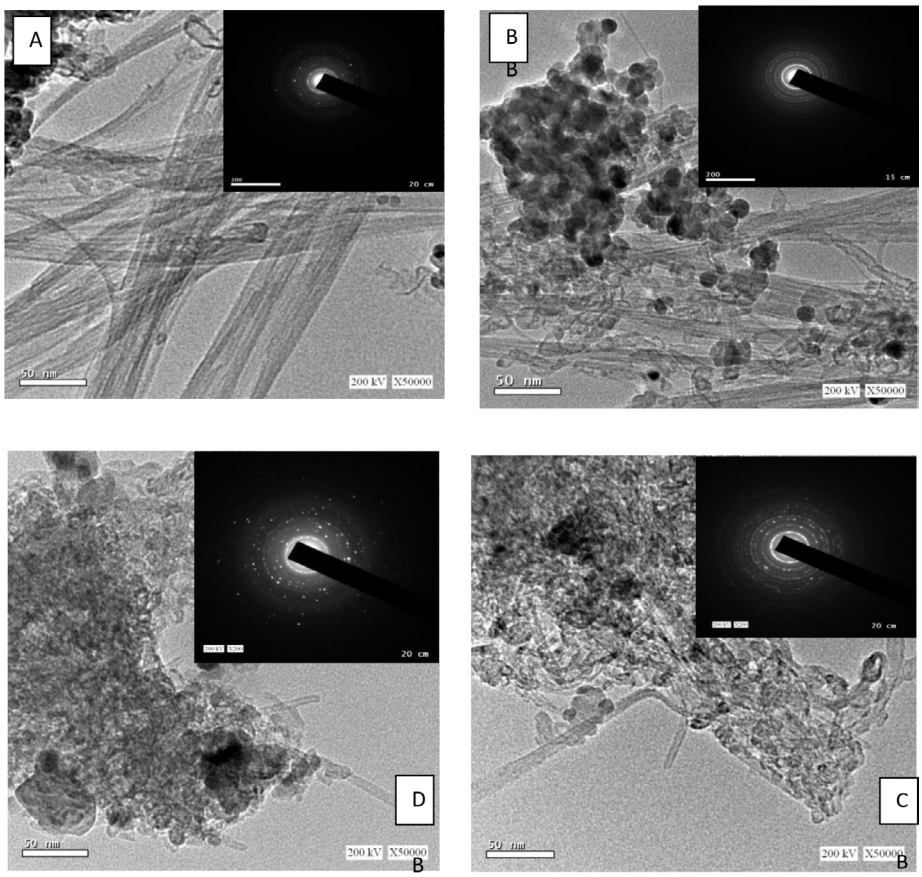

Fig. 2. HR-TEM Image (A) TNT-SWCNT (B) $TevAg_2$-SWCNT (C) $TevAg_6$-SWCNT and (D) $TevAg_2$-MWCNT, together with the corresponding SAED as insets.

an external diameter of approximately 8 nm and breaking CNT into shorter tubes. In comparison to rest of the samples, both $TevAg_6$-SWCNT and $TevAg_2$-MWCNT showed lower average diameters for Ag (3 nm) and TiO_2 (7 nm) nanoparticles.

Optical properties

The UV–visible diffuse reflectance (UV–vis DRS) of the $TevAg_6$--SWCNT and $TevAg_2$-MWCNT are depicted in figure S2. The DRS spectra of composite $TevAg_6$--SWCNT showed a band at 286 nm along with a broad one at 353 nm. They are correlated respectively, to π-π*transition in CNT and to anatase TiO_2. In addition to this,

Table 1. Zone inhibitions of different nanoparticle samples against *S. aureus* and *E. coli*

Sample Name	Zone of inhibition mm (*S. aureus*) 100ug/ml	Zone of inhibition mm (*E. coli*) 100ug/ml
Tev Ag_2 + MWCNT	23	25
Tev+ SWCNT	9	No result
Tev Ag_6 + SWCNT	30	45
Tev Ag_2 + SWCNT	22	25

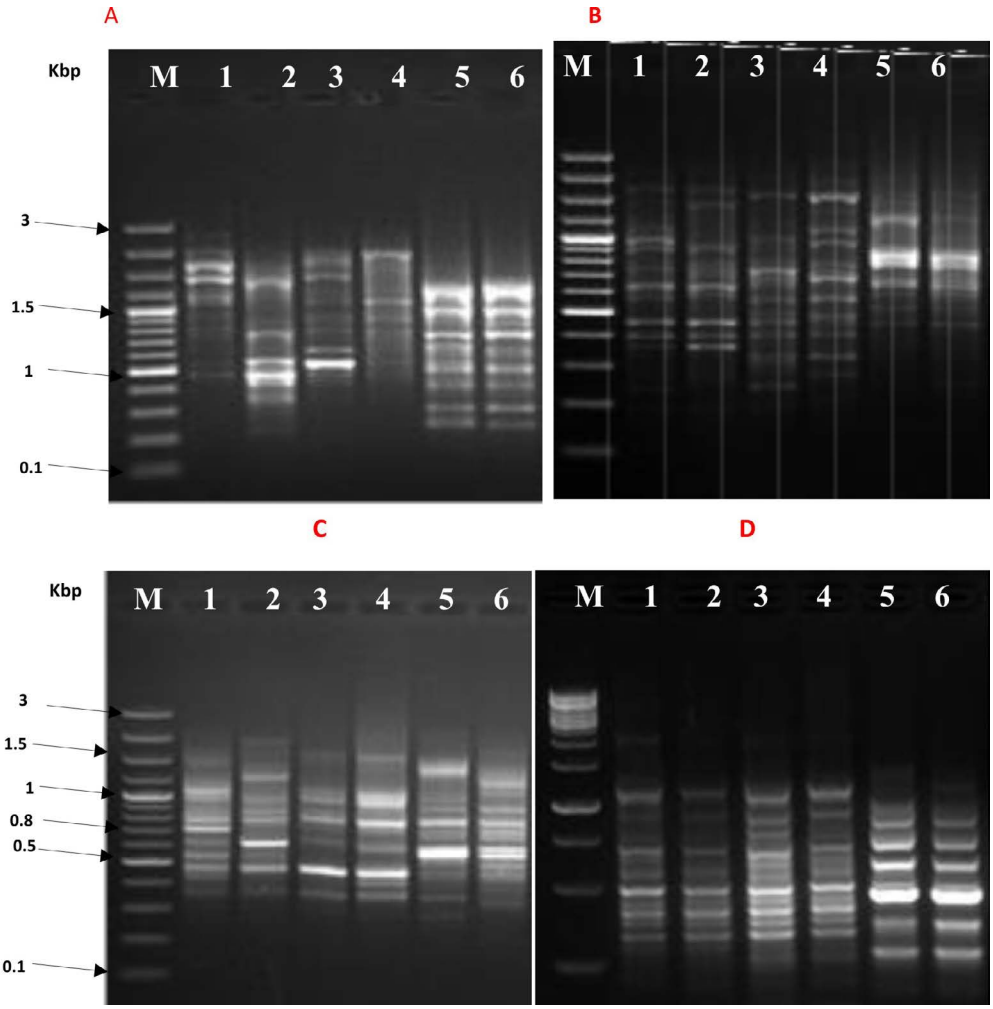

Fig. 3. RAPD PCR profile of *E. coli* by using 10 mer primer lane M: 100 pb plus marker, panel A, B, C, and D- lane 1: bacterial growth after 10 hr without nanoparticles, lane 2: bacterial growth after 10 hr with nanoparticles, lane 3: bacterial growth after 14 hr without nanoparticles, lane 4 : bacterial growth after 14 hr with nanoparticles, lane 5: bacterial growth after 18 hr without nanoparticles, lane 6: bacterial growth after 18 hr with nanoparticles.

the absorption spectra of $TevAg_2$-MWCNT and $TevAg_6$-SWCNT displayed similar absorption behaviour of Tev-SWCNT, but exhibit enhanced absorption towards visible-light region. This improved absorption is likely to be correlated with the strong interaction between Ag(TiO_2)and MWCNT(SWCNT) and the good dispersion; as committed previously employing XRD and TEM analysis. A narrow surface plasmon resonance band of about 440 nm was obtained in case of all Ag containing composites and thus reflecting the small size distribution of Ag nanoparticles. In order to determine the energy gap (Eg) we used the following approximation: $\alpha(hv) \propto (hv - Eg)n/2$ (Fig. S3). The Eg decreases in the following sequence: Tev-SWCNT (2.6)> $TevAg_2$-SWCNT (2.25)> $TevAg_6$-SWCNT (1.9)=$TevAg_2$-MWCNT(1.75).

Antibacterial activity

The antibacterial property of synthesized silver nanoparticles was investigated using agar well diffusion method by measuring the inhibition of bacterial growth against pathogenic strain of

Table 2. Zone inhibitions of positive control (amikacin or vancomycin) against *S. aureus* and *E. coli*

Control -	**Control** +
(mm)	(mm)
PAM	Van(+ve)
NA	13
Control -	Control +
(mm)	(mm)
PAM	Ami(-ve)
NA	15

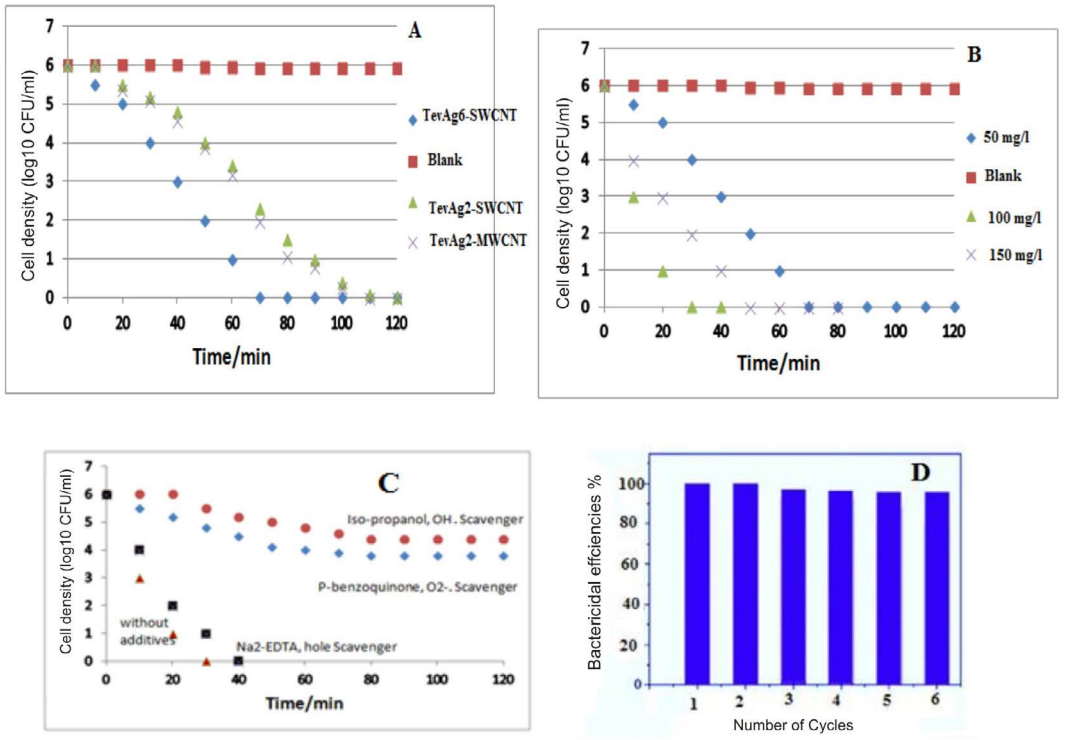

Fig. 4a. Disinfection efficiencies of *E. coli* by Ag containing photocatalysts under visible light irradiation. Dosages of different photocatalysts were 50 mg/L; **Fig. 4b.** Disinfection efficiencies of *E. coli* by $TevAg_6$-SWCNT photocatalyst under visible light irradiation as a function of varying the catalyst dosages; **Fig. 4c.** Disinfection efficiency of *E. coli* by 100 mg/L $Tevag_6$-SWCNT in the presence of different scavengers (5 mM Isopropanol, 5 mM P-benzoquinone, 5mM Na2-EDTA) under visible light irradiation; **Fig.4d**. Disinfection efficiency % of $TevAg_6$-SWCNT during different recycling process: reaction conditions: 30 min time cycle, 100 mg/l catalyst wt, 1 x 10^6 CFU/mL of *E.coli* cells

E. coli and *S. aureus. E. coli* is one of Gram negative bacterium and S. aureus is Gram positive one. The diameter of growth inhibition around each well in presence of nanocomposites is represented in Table 1. In negative control no zone of inhibition was observed. For the positive control, all the isolates, exhibited sensitivity toward either amikacin or vancomycin. The gram negative strains had higher antimicrobial activity 15 mm inhibition zone than gram positive strain 13 mm inhibition zone which was in accordance with the results reported by [35].

A remarkable inhibition zone was observed against *E. coli* for TevAg6-SWCNT with zone size of 40 mm, and the least (25 mm) was found with $TevAg_2$-SWCNT (MWCNT) samples. The size of inhibition zone produced by these samples was comparable to that of positive control (highest activity was 30 mm and least was 10 mm). On the other hand, the $TevAg_6$-SWCNT showed remarkable antimicrobial activity against *S. aureus* with 30mm zone size and moderate activity was observed in case of Tev Ag_2-SWCNT (22nm) and $TevAg_2$-MWCNT (23 mm).

Effect of nanocomposites on bacterial DNA

The effect of synthesized nanocomposites; particularly TevAg6-SWCNT that exhibited pronounced activity against both types of bacterial

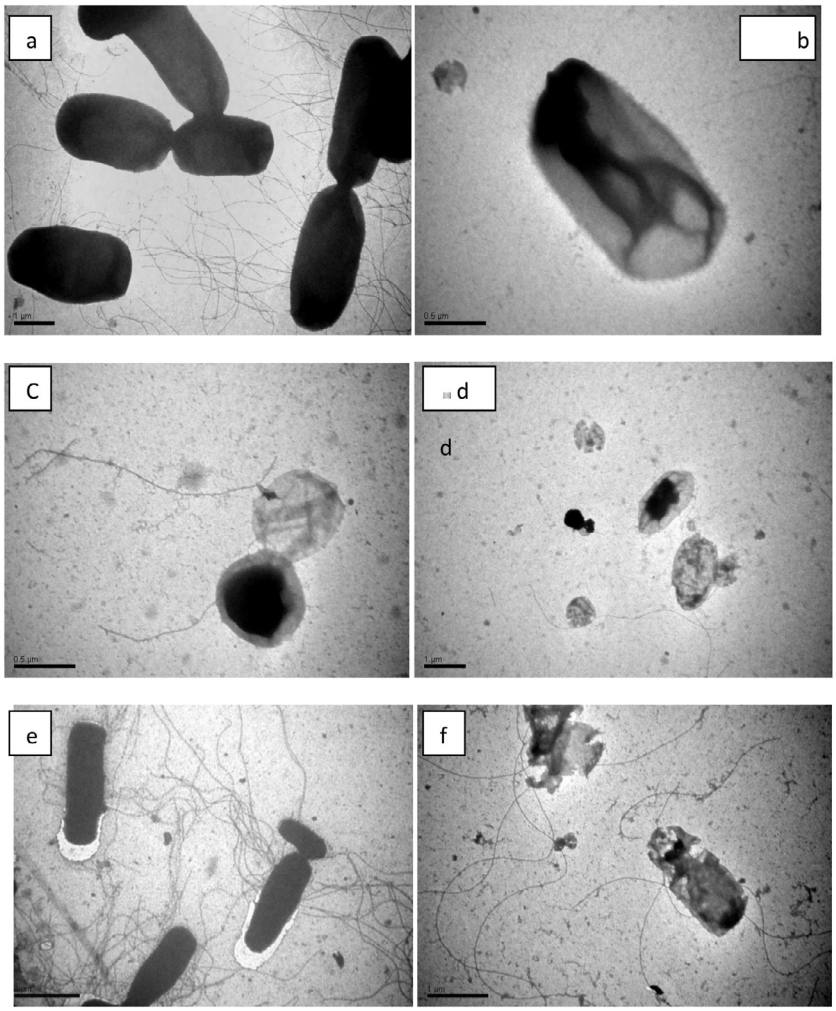

Fig. 5. TEM images of *S. aurues* (a-d) and *E. coli (e-f)* cells under dark and photocatalytic disinfection time when exposed to TevAg6-SWCNT catalyst at a dose of 100 mg/l: a) *S. aureus* after 10 min in dark (b) 10 h dark (c), 18 h dark (D), and 30 min under visible irradiation (e) *E. coli* after 10 min in dark (f) and after 30 min visible light irradiation.

strain, was investigated through the use of RAPD PCR (Fig. 3). Modification in intensity of bands and missed bands are likely to be the result of combined set of the following actions[36] (i) variations in oligonucleotide priming sites because of genomic reorganizations, probably due to point mutations; (ii) destruction of DNA through alterations in the binding sites the primer; and (iii) In the test organism, DNA polymerase interactions with damaged DNA. New DNA bands have also emerged because of accessibility of some oligonucleotide priming sites for oligonucleotide primers after structural changes or some alterations in the DNA sequence have also occurred due to mutations, large removals, and/or similar recombination[37].

The instability in genomic template associated with the efficiency of DNA repair, its replication and DNA damage level, could also be one of the reason for the appearance of new bands[38].

Disinfection activities of composites under visible illumination and stabilities

Generally, the illumination is appeared to markedly enhance the antibacterial activity of our nanocomposites to complete inhibition. Careful analysis has revealed that *E. coli* showed more susceptibility towards nanoparticles as compared to *S. aureus* either under dark or in light condition. The differences in response between 2 species are not clear known and it may represent the differences in metabolism, physiology or degree of contact. In addition, it also suggests that the basic mechanisms of nanoparticles toxicity might also vary depending upon their type as well as their physiochemical properties. It was observed in light control experiment, that irradiation of visible light did not show any toxic impact upon the bacterial cells as there was no decrease in viable bacterial population within the disinfection process (Fig. 4a). $TevAg_2$-MWCNT and $TevAg_2$-SWCNT suspensions could responsible for the complete deactivation of *E. coli* cells within 110 and 120 min respectively, whereas in case of TevAg6-SWCNT, the disinfection efficiency takes about 70 min. To check whether is there any Ag+ ions released during the disinfection process and thus affected the bactericidal activities, concentration of Ag+ ions was measured using ICP-AES after the exposure of $TevAg_6$-SWCNT sample to visible irradiation. Accordingly, we did not find any sufficient release of Ag+ ions (of detection limit ~ 20 ppb) i.e. its contribution in the inactivation process is insignificant. Fig. 4B summarizes the photocatalytic dosage effect of $TevAg_6$-SWCNT on *E. coli* growth parameters under visible light exposure. The photocatalyst, mentioned showed increased antimicrobial activity against *E. coli* bacteria at 100 mg L−1, a of dose, responsible for 100% CFU killing with in a period of 30 min, whereas increasing the dose into 150 mg/l showed a lower efficiency (100% in 50 min), comparatively. In addition, the exhibited interaction between TiO_2 and MWCNT was much more significant compared with SWCNT; as revealed from XRD, and TEM investigations, both of the nanocomposites ($TevAg_2$-SWCNT and $TevAg_2$-MWCNT) showed similar antibacterial activity against strains of *E. coli* and *S. aureus.* This strongly depicts the importance of Ti and C interaction which is achieved via exposed surface oxygen irrespective of type of CNTs. Accordingly, the recombination of photoinduced electrons and holes could be minimized by TiO_2-CNT heterojunction and exhibit more effective light absorption when there is incorporation of Ag nanoparticles at a loading of 6%.

It was observed that OH radicals was exhibited and affected bacterial degradation. Accordingly, for the diffusion of ·OH radical as a diagnostic tool, a small proportion of isopropanol (0.05 ml of $5x10^{-3}$ M) was incorporated in the form of scavenger while performing the agar well diffusion assay. There was significant reduction in the photocatalytic activity of the system after the addition of this agent, deciphering the lethal effect of ·OH (Fig.4C) on the bacterial cells. Furthermore, interaction of absorbed oxygen on CNT/TiO2 interface with electrons results in the formation of superoxide radicals (O2•−), which oxidized bacteria effectively as evaluated through the use of p-benzoquinone radical scavenger. No marked growth inhibitory activity against the test bacteria was observed employing the usage of Na_2-EDTA, in the form of hole scavenger. Although the $TevAg_2$-MWCNT showed lower Eg value as compared to $TevAg_6$-SWCNT, the enhanced activity of latter sample might be due to increased recombination rate of electrons and holes as depicted from PL measurements (not shown), which is probably responsible for their enhanced antimicrobial action. The recovery and reutilization of $TevAg_6$-

SWCNT nanocomposite for inactivation of cell throughout six consecutive cycles was examined under irradiation of visible light and the obtained results were shown in Fig.4D. Although, the bactericidal efficiencies of the photocatalyst was slightly reduced with repeated cycles (from 100% to 96% within 180 min). In case of *E. coli* cells complete inactivation of 1 × 106 CFU/mL was easily achieved through TevAg6-SWCNT within 30 min (Fig.4D). This result strongly suggested that $TevAg_6$-SWCNT owns a good potential for their repeated usage.

Mechanism of cell membrane damage

To understand deep insights of bacterial cell damage, images of TEM obtained via using a negative staining procedure was performed to determine the alterations in morphology of E. coli and cells of *S. aureus* during the process of inactivation (Fig. 5). Prior to the exposure of visible light irradiation, *S. aureus* cells posses an intact and smooth elliptical structure that changed when come in association with $TevAg_6$-SWCNT (Fig.5 c) into cylindrical shape through the mechanism of mutation. However, after exposure to visible irradiation to only 30 min,it has been found that the nanocomposites form cluster aggregates inside the bacterial cell. It can be observed that the part of Ag encapsulated inside TiO_2 is the one diffused inside the cell while CNT is extended outside the bacterial cell. On the other hand, no changes were observed with in 10 min in dark for *E. coli* acting as a control however, various pits appeared on the cell wall that gradually results in changes in its morphology after irradiation of visible light in 30 min (Fig.5 f). The cells become completely deformed and the damaged cell membrane generated ROS upon exposure to $TevAg_6$-SWCNT after 30 min treatment. Similar results have also been observed previously[39-40]. On the basis of the theory of hard and soft acids and bases, silver nanoparticles will exhibit superior affinity to interact with phosphorus and sulfur compounds[41]. The bacterial cell membrane is well known to posses large number of sulfur-containing proteins; that might act as a preferential site for the silver nanocomposites to interact with the cellular component of the bacterium such as with DNA[42]. Another reason for the interaction of the nanoparticles with bacteria is electrostatic interaction between bacterial membrane and nanocomposites. It has been also acknowledged that, at biological pH values, the entire bacterial surface are used to expose negative charges due to dissociation of carboxylic and phosphate moieties in the cell membrane[42]. The mechanism of Ag-nanoparticles release from the composites is affected by changes in pH. The effect of pH may explain why nanoparticles are more impacted on *E. coli* but not on *S. aureus* where after 18 hr *E. coli* can convert the media into highly acidic compared to *S. aureus*, which may lead to release more amount of effective nanoparticles. The silver nanoparticles synthesized using pH 9 show higher antibacterial activity (13mm) against *E. coli*. Small sized nanoparticles showed more antibacterial activity than large size particles because small sized particles affect surface area to adsorb large number of bacteria i.e. the smallest nanoparticles synthesized at pH 9 showed more antibacterial activity than large particles synthesized using original pH 4 and pH 5. The role of pH is crucial in controlling the size and shape of nanoparticles. It is quite clear that pH strongly affects the size and shape of the silver nanoparticles. We assume that the proton concentration affects conformational changes in the nitrate reducing enzymes present in the culture, which may change the morphology and size of the silver nanoparticles. The nanoparticles were not uniform in size and shape. Larger particles were formed at pH 4 and 5 with average particle size between 40 and 55 nm and smaller particles were formed at pH 8 and 9 with average particle size between 8 and 13 nm. The nanoparticles formed at lower pH (i.e., 4 or 5) were polydispersed with many different shapes such as pyramidal, spherical, and ellipsoidal. Some anisotropic nanostructures were formed with irregular contours, which indicate that the sample was composed of a large quantity of non-uniform nanoparticles. However, nanoparticles formed at pH 8 and 9 were more uniform spherical shape. These results show that the pH of the culture plays an important role in determining the morphology and shape of the silver nanoparticles. This variability in antimicrobial activity may be due to the variation in the surface area and shape of the nanoparticles. *E. coli* gram negative bacterium, seemed to be more adversely affected by the silver nano solution compared to the tested *S. aureus* which is gram

positive[43, 44]. Furthermore, the carbon nanotubes (insulator) embedded Ag nanoparticles and TiO_2 in the form of matrix, will enhance the existence of unlike charges on their cell membrane. On the basis of above mentioned facts it is possible to assume an electrostatic interaction between the nanocomposite and bacterial strain. Accordingly, based on the exposure of O_2•− and •OH on the surface of nanocomposite and configured reactive species, an invasion of either reactive species and/or nanocomposites inside the bacterial cytoplasmic membrane is expected and consequently mutation in DNA and K+ leakage has been achieved.

CONCLUSIONS

The synthesized Ag/TiO_2-CNTs have presented magnificent photo degradation towards *E. coli* and *S. aureus* bacterial strains under visible light irradiation in only 30 min. The inactivation mechanism was established based on performing some measurements including DNA, K+ leakage, TEM analysis of bacterial strains and Ag+ effect. These findings illustrated that due to unlike charges, the catalyst was found to stick upon the bacterial cell wall and therefore penetrate it. Consequently, the leakages of K+ ions along with DNA and protein mutations were explored as a result of deterioration of the bacterial cell. The characterization results; carried out using UV-Vis diffuse reflectance, reactive species and N_2 sorptiometry, have shown that the inactivation was supported by the generated ·OH and O_2•− ROS moieties upon irradiation of the catalyst surface along with low Eg values, high surface area, and the visible light capabilities of Ag/TiO_2 catalysts enhanced by the incorporation of CNTs.

ACKNOWLEDGEMENTS

This work is financially supported by the King Abdulaziz City for Science and Technology Research Grants Program # 11- NAN1694-10. The Authors are indebted to Egyptian petroleum research institute for allowing us to do the measurements of Raman, TEM-SAED, PL and N_2 sorptiometry in their labs. We are also thankful to Ms. Samreen, Researcher, Dept. of Agricultural Microbiology, AMU, Aligarh for the critical reading of the manuscript.

CONFLICT OF INTEREST

The authors declare that there is no conflict of interest.

AUTHORS' CONTRIBUTIONS

All authors listed have made a substantial, direct and intellectual contribution to the work, and approved it for publication.

FUNDING

This work was supported by the King Abdulaziz City for Science and Technology (Research Grants Program # 11- NAN1694-10.).

DATA AVAILABILITY

All datasets generated or analyzed during this study are included in the manuscript

ETHICS STATEMENT

This article does not contain any studies with human participants or animals performed by any of the authors.

REFERENCES

1. E.T. Thostenson, C. Y. Li, T. W. Chou, Compos. *Sci. Technol.*, 2005; **56**: 491–516.
2. K.T. Lau, C. Gu, D. Hui D, Composite Part B, 2006; **37**: 425–436.
3. A. Fujishima, K. Honda, *Nature*, 1972; **238**: 37–38.
4. I.K. Konstantinou, T.A. Albanis, *Appl. Catal. B Environ.*, 2004; **49**; : 1–14.
5. M. Muruganandham, N. Shobana, M. Swaminathan, *J. Mol. Catal. A Chem.*, 2006; **246**: 154–161.
6. M.H. Habibi, A. Hassanzadeh, S. Mahdavi, *J. Photochem. Photobiol. A Chem.*, 2005; **172**: 89–95.
7. C.H. Wu, *Chemosphere*, 2004; **57**: 601–608.
8. M. M. Mohamed, *Microporous & Mesoporous Materials*, 2008; **109**(1-3): 445-457.
9. W. D. Wang, P. Serp, P. Kalck, J. L. Faria, *J. Mol. Catal. A Chem.*, 2005; **235**: 194–199.
10. W.C. Oh, A.R. Jung, W. W. Ko, *J. Ind. Eng. Chem.*, 2007; **13**: 1208–1214.
11. W.C. Oh, M.L. Chen, *Bull. Korean Chem. Soc.*, 2008; **29**: 159–164.
12. W.D. Wang, P. Serp, P. Kalck, J.L. Faria, *Appl. Catal. B Environ.*, 2005; **56**: 305–312.
13. P.C. Ma, B.Z. Tang, J. K. Kim, *Carbon*, 2008; **46**: 1497–1505.
14. Y.J. An, W.S. Chung, J. Chang, H. C. Lee, Y. R. Cho, *Mater. Lett.*, 2008; **62**: 4277–4279.
15. M.M. Mohamed, M.S. Al-Sharif, Applied Catalysis B: *Environmental*, 2013; **142–143**: 432– 441.
16. M.M. Mohamed, *Microporous & Mesoporous*

Materials, 2011; **142**: 130.
17. S. Zaki, M. El Kady, D. Abd-El-haleem, *Material Research Bulletin*, 2011; **46**: 1571-1576.
18. I. Sondi, B. Salopek-Sondi, *J. Colloid Interface Sci.*, 2004; **275**: 177–182.
19. M. Ansari, H. Khan, K. Aijaz, A. Kaleem, A Mahdi, P. Ruchita, S Cameotra, *Journal of Basic Microbiology*, 2014; **54**: 905-915.
20. T.N. Kim, Q.L. Feng, J.O. Kim, J. Wu, H. Wang, G.C. Chen, F.Z. Cui, *J. Mater. Sci. Mater. Med.*, 1998; **9**: 129-135.
21. M. Bellantone, H.D. Williams, L.L. Hench, Antimicrob. *Agents Chemother.*, 2002; **16**: 1940-1947.
22. S.Y. Kwak, S.H. Kim, S.S. Kim, *Environ. Sci. Technol.*, 2001; **35**: 2388-2393.
23. M. A. Fox, M. T. Duby, *Chem. Rev.*, 1993; **93**: 341-348.
24. K. Sunada, T. Watanabe, K. Hashimoto, *Environ. Sci. Technol.*, 2003; **37**: 4785-4790.
25. P.C. Maness, S. Smolinski, D.M. Blake, Z. Huang, E.J. Wolfrum, W.A. Jacoby, *Appl. Environ. Microbiol.*, 1999; **65**: 4094-4099.
26. A. Henglein, *J. Phys. Chem.*, 1993; **97**: 5457-5465.
27. A.P. Alivisatos, *J. Phys. Chem.*, 1996; **100**: 13226-13233.
28. G.Fu, P.S. Vary, C.T. Lin, *J. Phys. Chem. B.*, 2005; **109**: 8889-8894.
29. S-Y. Wang, S-Y. Wu, G. Thottapilly, R. D. Locy, N. K. Singh, *J. Biosci, Bioeng.*, **92**: 59-66.
30. J.G. K. Williams, A.R. Kubelik, K.J. Livak, J.A. Rafalski, S. V. Tingey, *Nucleic Acids Res.*, 1990; **18**: 6531-6535.
31. J.G.K. Williams, M.K. Hanafey, J.A. Rafalski, S.V. Tingey, Methods Enzymo., 1993; **218**: 704-740.
32. Torres A, Garedew A, Schmolz E, Lamprecht I, *Thermochim Acta.*, 2004; **415**: 107.
33. M.M. Mohamed**,** M.S. Al-Sharif, *Materials Chemistry and physics*, 2012; **136**: 528-537.
34. G.A. Tompsett, G.A. Bowmaker, R.P. Cooney, J.B. Metson, K.A. Rodgers, J.M. Seakins, *J. Raman Spectrosc*., 1995; **26**: 57-62.
35. Woo Kyung Jung, Hye Cheong Koo, Ki Woo Kim, Sook Shin, So Hyun Kim, and Yong Ho Park. *Applied and environmental microbiology. apr.*, 2008; **74**(7): 2171 .
36. K.-H. Choi, N. Duraisamy, N.M. Muhammad, I. Kim, H. Choi, J. Jo, Applied Physics A 107 (2012) Issue 3, 715-722.
37. N.L. Kovtyukhova, T.E. Mallouk, L. Pan, L.E.C. Dickey, *J. Am. Chem. Soc.*, 2003; **125**: 9761-9769.
38. P. Wilhelm, D. Stephan, *Journal of Photochemistry and Photobiology A: Chemistry*, 2007; **185**: 19–25.
39. S. Niakan, M. Niakan, S. Hesaraki, M.R. Nejadmoghaddam, M. Moradi, M. Hanafiabdar, *Microbiol.*, 2013; **6**: e8341-e8346. DOI: 10.5812/jjm.8341.
40. S.J. Kazmi, M.A. Shehzad, S. Mehmood, M. Yasar, A. Naeem, A. S. Bhatti, *Sensors and Actuators A*, 2014; **216**: 287–294.
41. M.D. Giulio, S.D. Bartolomeo, E.D. Campli, S. Sancilio, E. Marsich, A. Travan, A. Cataldi, L. Cellini, *Int. J. Mol. Sci.*, 2013; **14**: 13615–13625.
42. S. Sakthivel, M. Janczarek, H. Kisch, *J. Phys. Chem. B.*, 2004; **108**: 19384-19389.
43. Nayak R.R., N. Pradhan, D. Behera et al., "Green synthesis of silver nanoparticle by Penicillium purpurogenum NPMF: the process and optimization," *Journal ofNanoparticle Research*, 2011; **13**(8): 3129–3137.
44. Kethirabalan Chitra and Gurusamy Annadurai Antibacterial Activity of pH-Dependent Biosynthesized Silver Bio. Med. Research International Volume 2014, Article ID 725165, 6 pages Nanoparticles against Clinical Pathogen.